Zero Voltage Vector Sampling Method for PMSM Three-Phase Current Reconstruction Using Single Current Sensor

Yongxiang Xu, *Member, IEEE*, Hao Yan, *Student Member, IEEE*, Jibin Zou, *Senior Member, IEEE*, Baochao Wang, *Member, IEEE*, and Yunhui Li

***Abstract*—For the purpose of reducing cost and volume, techniques of reconstructing three-phase currents through a single current sensor have been reported for permanent magnet synchronous motor vector control system. In existing studies, the reconstruction precision is largely affected by the dead zones in space vector PWM plane, which requires additional efforts to compensate the dead zones either by modifying pulse width modulation (PWM) modulation strategy or by phase-shifting of PWM signal. In this paper, a novel zero voltage vector sampling method (ZVVSM) is proposed, which can move the current reconstruction dead zones in low modulation region and sector boundary regions toward the outline of the space vector hexagon without modifying PWM signal. By arranging the single current sensor at a novel position, the proposed method is able to sample current in two zero voltage vectors (ZVV). ZVVSM avoids the complicated algorithms as well as the increase of the switching times, so that it is beneficial to the PMSM drive performance. The proposed method is validated by both simulation and experiments.**

***Index Terms*—Dead zone, permanent magnet synchronous motor (PMSM), phase current reconstruction, single current sensor, voltage vector, zero voltage vector sampling method (ZVVSM).**

I. Introduction

PERMANENT-MAGNET synchronous motors (PMSMs) are widely used in industrial applications owing to their merits such as high efficiency, high precision, and high reliability [1]–[4]. Conventionally, PMSM drive requires at least two current sensors [5] and a position sensor [6]–[8]. To reduce cost and volume, as well as to increase reliability in hostile environment [9], technical trends move toward driving PMSM with fewer sensors. Position-sensorless control has been widely studied and implemented in lots of industrial applications such as fans and pumps. In [10] and [11], the current sampling upon short voltage vectors have been tackled in research on position-sensorless drives, which use motor phase current derivatives. As for current, studies to reconstruct three-phase currents using single current sensor have been undertaken as well [12]–[28].

Most of the methods install the single current sensor on dc bus. The steady-state relationships between the dc-link current and the phase currents for various inverter switch states have been reported in [12]. However, this method introduces dead zones, where steady-state conditions can hardly be satisfied. The dead zones are analyzed in [13], where it is identified that the dead zones are located in the areas, where the output voltage vector is in the low-modulation region, and space-vector sector boundary region. To reduce the current reconstruction dead zones, different compensation methods are proposed, which are based on modifying pulse width modulation (PWM) modulation, measurement-vector insertion, and phase shifting.

In [14] and [15], the modified PWM modulation strategies for reconstructing the three-phase currents from the dc-link current are given. A new modulation technique that can reduce the current distortion and extend the current reconstruction range for a three-phase inverter using only dc-link sensor is also proposed in [16]. The proposed PWM technique is a hybrid method that consists of space vector modulation method and the PWM method without using null switching states. Moreover, state observer algorithms are adopted to reconstruct the phase currents [17], [18].

Other research work is reported on the measurement-vector insertion method (MVIM). In [19], the proposed method involves the injection of voltage signals at the carrier frequency for reconstructing the phase currents in PWM inverters using a single current sensor in the dc-link. In [20] and [21], the MVIM is adopted to reconstruct all three inverter phase currents using a single current sensor.

Besides, the switching-state phase shift method is proposed to minimize the dead zones in [22]. In [23], a technique for predicting phase currents in vector-controlled inverters. The proposed method predicts the currents measured at the fixed sampling points from those measured in the dc link and the PWM patterns of voltage outputs. Some other methods, like the overmodulation method, tri-state PWM, and Luenberger observers are all used in the single current sensor techniques [24]–[26]. A six-phase current reconstruction scheme for dual traction inverters

Manuscript received March 14, 2016; revised June 13, 2016; accepted June 28, 2016. Date of publication July 7, 2016; date of current version February 2, 2017. This work was supported in part by the 973 Program under Grant 2013CB035605, in part by the National Natural Science Foundation of China under Grant 51437004, and in part by the National Natural Science Foundation of China under Grant 51577036. Recommended for publication by Associate Editor B. Wang. *(Corresponding author: Hao Yan).*

Y. Xu, H. Yan, J. Zou, and B. Wang are with the School of Electrical Engineering, Harbin Institute of Technology, 150001 Harbin, China (e-mail: xuyx@hit.edu.cn; yanhaohit@yahoo.com; zoujibin@hit.edu.cn; baochao.wang@hit.edu.cn).

Y. Li is with the Changchun Institute of Optics, 130000 Changchun, China (e-mail:liyunhui_ciomp@126.com).

Color versions of one or more of the figures in this paper are available online at http://ieeexplore.ieee.org.

Digital Object Identifier 10.1109/TPEL.2016.2588141

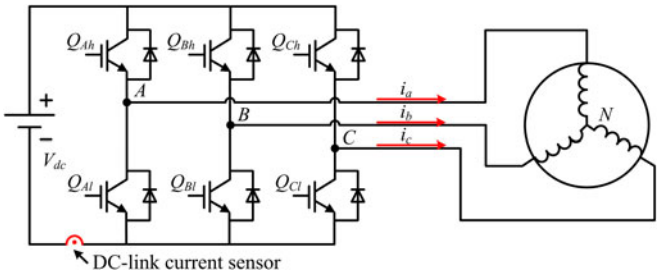

Fig. 1. Schematic diagram of a conventional PMSM drive.

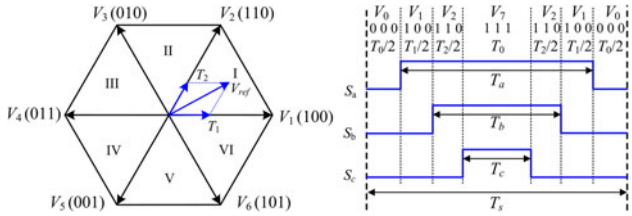

Fig. 2. Reference voltage in Sector I and its seven-segment PWM waveform in the conventional SVPWM algorithm.

with a single dc-link current sensor is proposed in [27]. In [28], a dc-link current sensor is used to implement a novel position sensorless PMSM drive. These compensation methods affects normal PWM signal and results in negative impact on motor control performance or complexity for implementation.

After analyzing the existing single current sensor techniques, the current reconstruction dead zones in the low-modulation region and sector boundary regions can be removed and the working performance of the PMSM can be improved. This paper proposes a novel single current sensor technique for three-phase PMSM drive. This proposed method is implemented by changing the installation position of the single current sensor and sampling the current during the zero voltage vectors, namely zero voltage vector sampling method (ZVVSM). This paper is organized as follows. At first, in Section II, the principles as well as the dead zones of existing methods using a dc-link current sensor are introduced. Then, the proposed ZVVSM and dead zone analysis are introduced in Section III. The closed loop control system based on the proposed method is established and the MATLAB/Simulink simulation results are included in Section IV. Section V presents the experimental setup and results for further validation. At last, Section VI gives the conclusion.

II. Three-Phase Current Reconstruction Method Using a DC-Link Current Sensor

In the conventional phase current reconstruction method [12], the single current sensor is installed on the dc link. The principle and the dead zones of this method are introduced in this section, which is used for comparison.

Fig. 1 shows the schematic diagram of single-sensor PMSM drive. In general, the motor is fed by a voltage-source PWM inverter that consists of six power switches and six freewheeling diodes. The voltage-source PWM inverter switches have eight combinations that form six active voltage vectors and two zero voltage vectors across its terminals. Generally, the eight generated switching states can be expressed together as the voltage space vector V_i, $i \in \{0, 1, 2, \ldots, 7\}$, as shown in Fig. 2, as well as its seven-segment PWM waveform in the conventional SVPWM algorithm. In Fig. 2, T_s is the PWM period, T_A, T_B, and T_C are the conduction interval of three phases.

As shown in Fig. 2, during steady state of the active voltage vector periods, the switching states as well as the current circuits remain unchanged, so there is a certain relationship between the phase currents and the dc-link current. By analyzing the eight voltage vectors and the current circuits, the relationship between

TABLE I
Relationship Between the Phase Currents and the DC-Link Current at Different Voltage Vectors

V_i	V_0	V_1	V_2	V_3	V_4	V_5	V_6	V_7
$S_{\rm abc}$	000	100	110	010	011	001	101	111
$i_{\rm dc}$	0	$+i_a$	$-i_c$	$+i_b$	$-i_a$	$+i_c$	$-i_b$	0

the phase currents and the dc-link current is summarized in Table I. In this table, $S_{\rm abc}$ are the switching states of the inverter switches and the eight voltage vectors are formed by them. In the switching states, only the switching functions of upper switches are used to define them. For example, $S_{\rm abc} = (100)$, generating the voltage vector V_1, means $Q_{\rm Ah} = {\rm on}$, $Q_{\rm Bh} = {\rm off}$, and $Q_{\rm Ch} = {\rm off}$. Furthermore, the positive sign $(+)$ indicates the inflow of the phase currents and the negative sign $(-)$ indicates the outflow of the phase currents.

According to this relationship between the phase currents and the dc-link current, the three-phase currents can be reconstructed by measuring the dc-link current. Taking the voltage vector in Sector I, for example, the reference voltage vector is generated by four switching states, $S_{\rm abc} = (000)$, (100), (110) and (111) in a PWM period T_s. Then, by measuring the dc-link current, the phase currents $+i_{\rm a}$ and $-i_{\rm c}$ can be obtained under the two switching states $S_{\rm abc} = (100)$ and (110), respectively. Since the phase currents meet the following (1), the phase current i_b can be calculated as well. Hence, the phase currents can be reconstructed by measuring the dc-link current under active voltage vectors in a PWM period and this method can be called active voltage vector sampling method. The relationship between the phase currents and the dc-link current at different voltage vectors is shown in Table I

$$i_a + i_b + i_c = 0. \tag{1}$$

Nevertheless, it is required a minimum duration for the voltage vectors to realize precise sampling in the actual situation [12]. Due to this restriction, there are two areas where currents cannot be measured, which are red and blue in Fig. 3. In these two areas, which are low-modulation region and sector boundary region, the duration of active voltage vectors is too short to sample currents as the current waveforms contain disturbances related to transistor switching. So there are large current reconstruction dead zones that can limit the motor's operation range. Although some improved methods have been proposed to narrow the dead zones, these methods can reduce the performance of the motor drive system and make the algorithms complex.

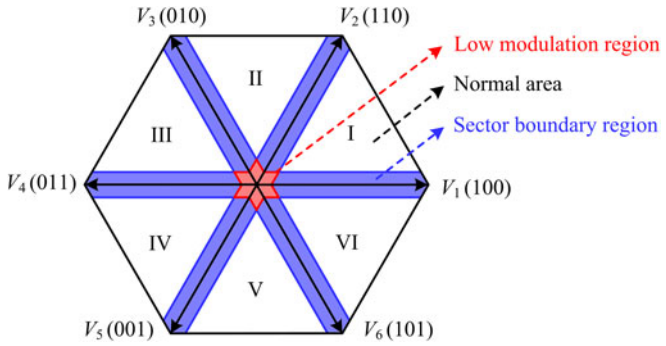

Fig. 3. Normal working area and current reconstruction dead zones using the phase current reconstruction method with a dc-link current sensor.

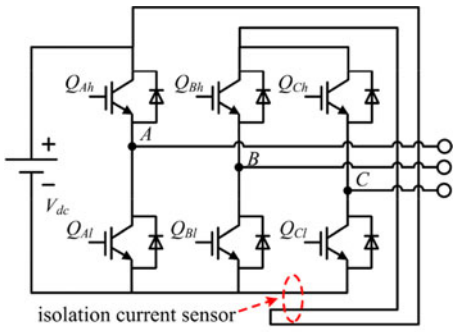

(a)

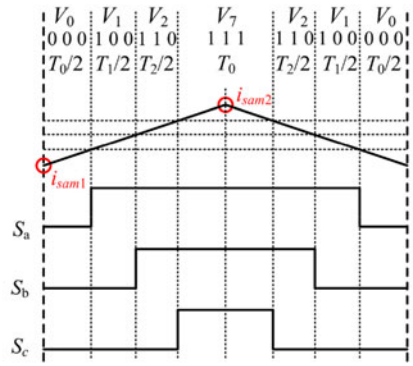

(b)

Fig. 4. Circuit topology and sampling points of the ZVVSM. (a) Circuit topology and the installation of the single hall-effect current sensor. (b) Sampling points in a PWM cycle.

III. Zero Voltage Vector Sampling Method (ZVVSM)

Based on the principle of phase current reconstruction methods, this paper proposes a novel method named ZVVSM. The circuit topology and the sampling points of the ZVVSM are illustrated in Fig. 4(a). In this proposed method, the isolated hall-effect current sensor is installed to detect the sum of the two currents flowing through the inverter bridges. Moreover, as Fig. 4(b) illustrates, the current sensor is sampled during the two zero voltage vectors and the triangular wave at the top presents the PWM carrier.

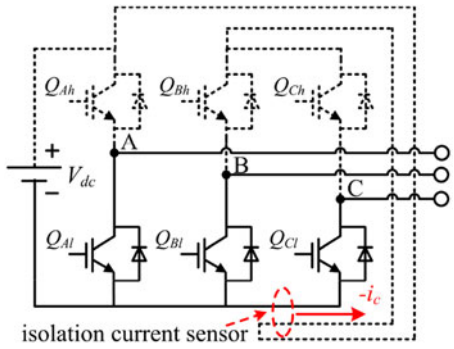

(a)

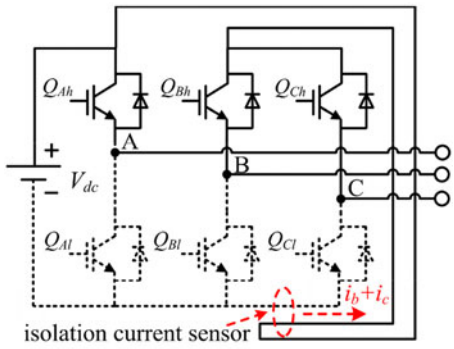

(b)

Fig. 5. Paths of the current flow at two zero voltage vectors. (a) V_0 (000). (b) V_7 (111).

A. Basic Working Principle of ZVVSM

In this proposed method, the phase current can be reconstructed by sampling the current during the zero voltage vectors. To further explain the method in detail, taking the voltage vector in the space vector hexagon, for example, there are two zero voltage vectors V_0 (000) and V_7 (111) in a PWM cycle, so the single current sensor is sampled twice in each PWM cycle. The sampling interval is half a PWM cycle, which may reduce the dynamics of current control [29]. In this paper, the positive sign (+) indicates the inflow of the phase currents and the negative sign (−) indicates the outflow of the phase currents.

Fig. 5(a) illustrates the path of the current flow when the output voltage vector is V_0 (000). Here, the load current freewheels through the lower switches, and the current sensor is read as

$$i_{\mathrm{sam}V} = i_c \tag{2}$$

where $i_{\mathrm{sam}V}$ is the sample value of the current sensor at the PWM carrier valleys. This sampling is the first sampling and occurs at the beginning of the PWM cycle. Then, Fig. 5(b) shows the path of the current flow when the output voltage vector is V_7 (111). Different from the former switching state, the current freewheels through the load and the upper switches. And the sample value of the current sensor is

$$i_{\mathrm{sam}P} = i_b + i_c \tag{3}$$

where $i_{\mathrm{sam}P}$ is the sample value of the current sensor at the PWM carrier peaks. This sampling is the second sampling and

TABLE II
RELATIONSHIP BETWEEN THE SAMPLING CURRENTS AND THE PHASE CURRENTS UNDER ZVVSM

Voltage Vectors	V_0 (000)	V_7 (111)
Sampling Currents	i_c	$i_b + i_c$

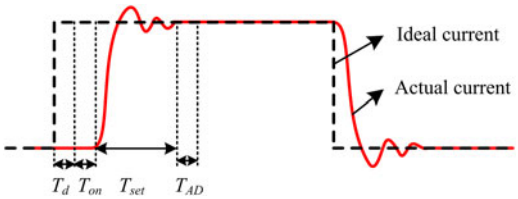

Fig. 6. Actual current and ideal current in the ZVVSM.

occurs at the middle of the PWM cycle. In summary, the relationship between the sampling currents and the phase currents is shown in Table II. According to this table, the phase currents i_a and i_c can be obtained if the current sensor is sampled during the two zero voltage vectors V_0 (000) and V_7 (111).

Since the three-phase windings are Y-connected in the PMSM and the phase currents meet the (1). The phase current i_b can be calculated as well. As a result, the three-phase currents can be reconstructed during a PWM period, which are expressed as

$$\begin{cases} i_a = -i_{\mathrm{sam}P} \\ i_b = i_{\mathrm{sam}P} - i_{\mathrm{sam}V} \\ i_c = i_{\mathrm{sam}V} \end{cases} \tag{4}$$

B. Minimum Reliable Current Measurement Time $T_{\min}$

In the actual situation of current based on the ZVVSM, illustrated in Fig. 6, the current cannot follow the applied voltage immediately due to the motor inductance and it takes some time, denoted as T_{set}, to reach the steady state. Moreover, the A/D converter of digital signal processor (DSP) needs an extra conversion time after reaching steady state, denoted as T_{AD}. In addition, the total switching device turn-on delay time and the dead zone time between the two switching devices in one bridge leg for protection should be taken into consideration as well, which are denoted as T_{on} and T_d, respectively.

Based on these factors, it is required a minimum duration for the zero voltage vectors to realize precise sampling. Moreover, this minimum reliable current measurement time, denoted as $T_{\min}$, should satisfy the following inequality:

$$T_{\min} \geq T_{\mathrm{set}} + T_{\mathrm{AD}} + T_{\mathrm{on}} + T_d. \tag{5}$$

By measuring the signal settling time T_{set} and querying the registers of DSP as well as the datasheet of IGBT, the four parts of $T_{\min}$ are obtained: $T_{\mathrm{set}} = 2.7$ μs, $T_{\mathrm{AD}} = 0.16$ μs, $T_{\mathrm{on}} = 0.36$ μs, and $T_d = 0.85$ μs. So, the minimum value of $T_{\min}$ is 4.07 μs. It is necessary to leave some margin to ensure that the reliable current measurement. As a result, we set the factor $T_{\min}$ as 5 μs in this paper.

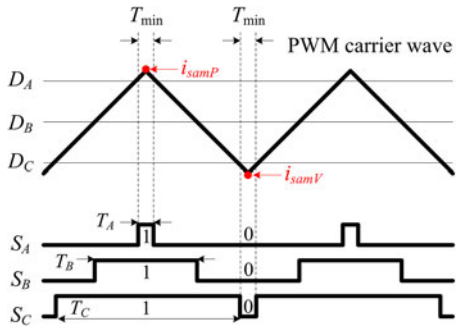

Fig. 7. Minimum reliable current measurement time $T_{\min}$ and its duty cycle limitation under ZVVSM.

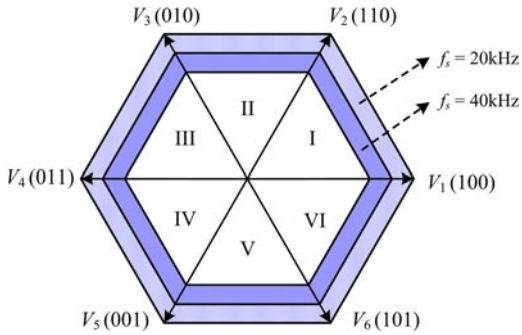

Fig. 8. Current reconstruction dead zones of ZVVSM and the relationship with the PWM frequency f_s.

$T_{\min}$ is like a restriction on the duration of the voltage vectors or the duty cycle of PWM, therefore, to ensure the reliable current sampling, $T_{\min}$ should be set as a reasonable value in the algorithms in advance. Then, $T_{\min}$ determines the minimum duration of the two zero voltage vectors V_0 and V_7 in SVPWM. Fig. 7 illustrates this relationship between $T_{\min}$ and its duty limitation under ZVVSM, where D_A, D_B, D_C are the duty cycles of the three phases. The single current sensor is sampled at the valleys and peaks of the PWM carrier wave and the sampling results are determined by the current sensor outputs at these sampling instants. However, the factor $T_{\min}$ just limits the sampling range, where the sampling points are located. As a result, if the factor $T_{\min}$ is set up reasonably and the motor is not operated in the dead zone region, the sampling results will not be influenced by $T_{\min}$.

C. Dead Zone Analysis

Similar to other phase current reconstruction methods, ZVVSM also has the current reconstruction dead zone. In this method, the zero voltage vectors must maintain enough time to guarantee the current sampled. Since the duration of zero voltage vectors will be reduced with the amplitude of voltage vector increasing, the current cannot be sampled successfully when the amplitude of voltage vector is too large. As a result, there will be a current reconstruction dead zone, which is illustrated in Fig. 8 and marked with shadow area. In this figure, it is obvious that there are no dead zones in the low-modulation region and sector boundary region compared with the single dc-link

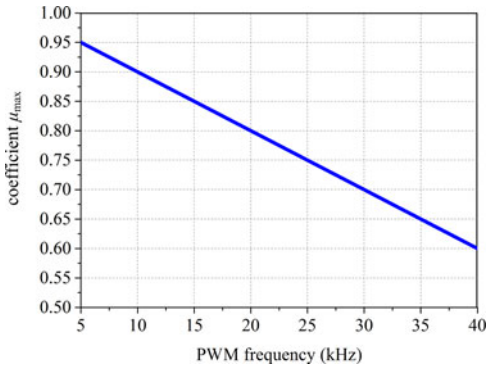

Fig. 9. Relationship between the maximum active voltage vector proportionality coefficient and the PWM frequency f_s under ZVVSM; $T_{\min} = 5\ \mu$s.

current sensor method. Furthermore, ZVVSM does not increase the switching times of the inverter during each PWM cycle, so the switching loss of the inverter will not increase.

To further study the relationship between the duration of zero voltage vectors and the current reconstruction dead zone, a proportionality coefficient μ is introduced. It is the ratio of active voltage vector duration to the PWM period T_s, expressed as follows:

$$\mu = \frac{T_s - T_0}{T_s}. \tag{6}$$

In the conventional Space Vector Modulation algorithm, the duration of zero voltage vector T_0 should be equally distributed to the switching states $S_{\rm abc} = (000)$ and (111). Since duration of the two zero voltage vectors should exceed the minimum reliable current measurement time $T_{\min}$ discussed earlier, the duration of zero voltage vector need satisfy the inequality

$$T_0 \geq 2T_{\min}. \tag{7}$$

Then, by substitution of the inequality into (6), the maximum active voltage vector proportionality coefficient, $\mu_{\max}$, can be computed as follows:

$$\mu_{\max} = \frac{T_s - 2 \cdot T_{\min}}{T_s} = \frac{1/f_s - 2 \cdot T_{\min}}{1/f_s} = 1 - 2f_s \cdot T_{\min}. \tag{8}$$

More, the maximum voltage vectors output of ZVVSM can be expressed as

$$V_{\max 1} = \frac{2}{3} V_{\rm dc}(1 - 2f_s \cdot T_{\min}). \tag{9}$$

It can be concluded that the proportionality coefficient $\mu_{\max}$ decreases when the PWM frequency f_s or the minimum reliable current measurement time $T_{\min}$ increases. Generally, the interval $T_{\min}$ is a constant, so the maximum active voltage vector proportionality coefficient $\mu_{\max}$, as well as the effective operation region of the voltage vector, will decrease with the PWM frequency increasing. Fig. 9 shows the relationship between the maximum active voltage vector proportionality coefficient and the PWM frequency f_s under ZVVSM. In this figure, it is obvious that the maximum active voltage vector, as well as the effective operation region of the voltage vector, will decreases with the PWM frequency increasing. As illustrated in Fig. 8, the effective operation region shrinks inward with the PWM frequency increasing. The shadow region indicates the dead zones of the ZVVSM at different frequencies.

TABLE III
PMSM DRIVE PARAMETERS

Parameters	Quantity
Winding resistance (R_a)	0.62 Ω
Winding inductance (L_a)	0.28 mH
Back EMF coefficient (K_e)	$0.1103\ V/(\text{rad}/s)$
Moment of inertia (J)	0.82 g.m^2
Number of pole pairs (p)	4
DC-link voltage ($V_{\rm dc}$)	60 V
Rated torque (T_N)	5 N.m
Rated speed (n_N)	$1000\ \text{r}/\ \text{min}$

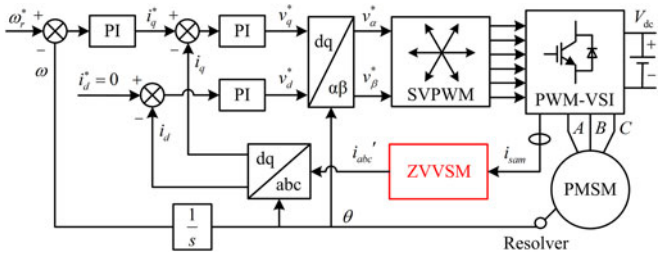

Fig. 10. PMSM control strategy based on ZVVSM.

Therefore, compared to the dc-link current reconstruction method, ZVVSM is available in the low-modulation region and sector boundary region, which avoids lots of the complicated algorithms to improve the dead zones. After calculating the areas of dead zones of the typical single dc-link current sensor method [24], ZVVSM does not reduce the areas of dead zones. It moves the dead zones toward the outline of the space vector hexagon. In general, ZVVSM provides a new solution for the single current sensor control strategy.

IV. SIMULATION RESULTS

To corroborate the novel phase current reconstruction method, the MATLAB/Simulink environment has been used for the simulation. More, the load of the three-phase PWM-VSI is a PMSM and the motor parameters are reported in Table III. The table includes the parameters of the actual experimental drive, which are also used for the establishment of simulation model. The PWM-VSI is controlled with 10-kHz switching frequency of the power semiconductor devices and a 60-V dc-link nominal voltage.

Fig. 10 shows the PMSM control strategy based on ZVVSM. In this control strategy, the PMSM is driven by a speed and current double closed loop. The outputs of single current sensor are sampled based on ZVVSM and the three-phase currents are reconstructed. Furthermore, the reconstructed phase currents are transformed to the d–q synchronous rotating frame, i_d and i_q, which are the feedback current signals of the current loops. Other algorithms in this control strategy are the same as the conventional double-close-loop PMSM control strategy.

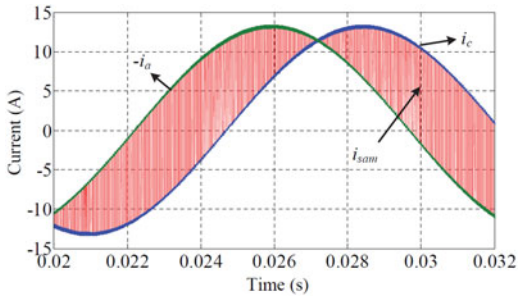

Fig. 11. Single current sensor output $i_{\rm sam}$ and the actual phase currents—i_a and i_c (Simulation results).

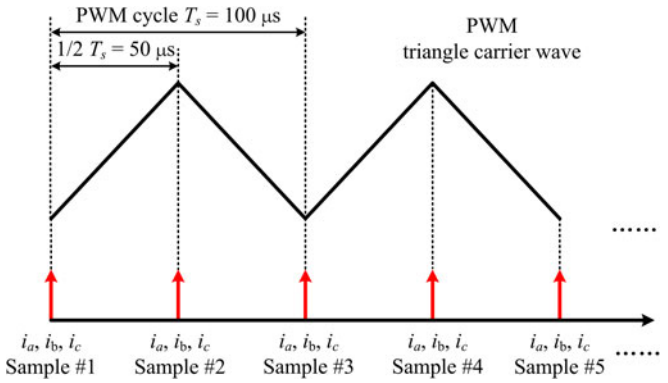

Fig. 12. Sampling principle and discretization of the actual phase currents in the simulation.

Fig. 11 shows the simulation results of the current sensor output $i_{\rm sam}$ and the actual phase currents $-i_a$ and i_c. It can be observed that the single current sensor output contains the current information of phase A and C. The two envelope curves of the single current sensor output are consistent with the phase currents $-i_a$ and i_c.

The actual three-phase currents, illustrated in Fig. 13(a), are continuous and contain the ripple components. However, based on the ZVVSM, the reconstructed results are discrete values. Therefore, to avoid the effect of the ripple components on the results of the proposed algorithms, the discrete ZVVSM outcomes should be compared with discretized values of actual currents. In the simulation, the actual phase currents are discretized by computing the mean current value for each PWM cycle. Fig. 12 shows the sampling principle of the actual phase currents in the simulation. The continuous actual phase currents are sampled twice in a PWM cycle, which are occurred at the valleys and peaks of the PWM triangle carrier wave. Then, the twice sampling results are averaging to get the mean value during each PWM period as the discretized values of actual currents, which are illustrated in Fig. 13(b).

The reconstructed phase currents based on ZVVSM are illustrated in Fig. 14. From this figure, it can be concluded that the ZVVSM can reconstruct the three-phase currents. Nevertheless, there are still current estimation errors, shown in Fig. 15, which are the difference value between the Phase A currents in the discrete ZVVSM outcomes in Fig. 14 and the discrete actual phase currents in Fig. 13(b). Compared with the value of

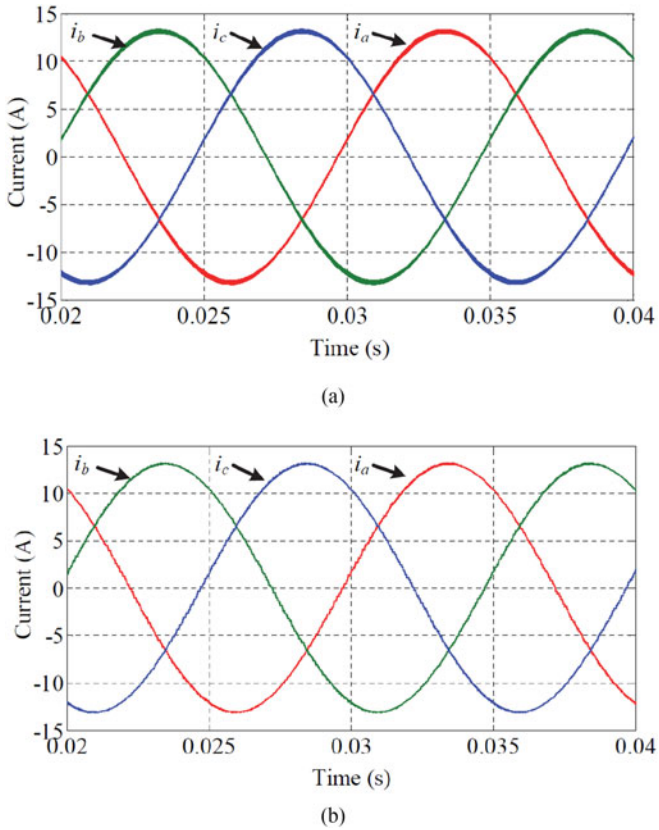

Fig. 13. Actual phase currents as well as their discretized values under ZVVSM (simulation results). (a) Continuous values of actual phase currents. (b) Discretized values of actual phase currents.

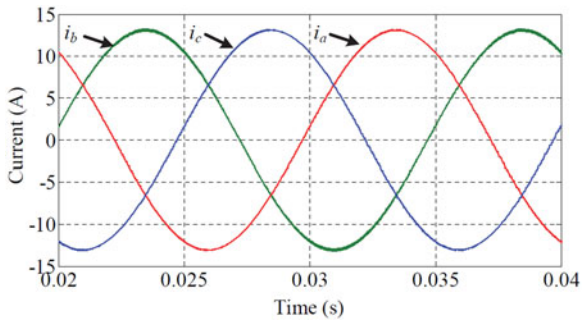

Fig. 14. Reconstructed phase currents under ZVVSM (simulation results).

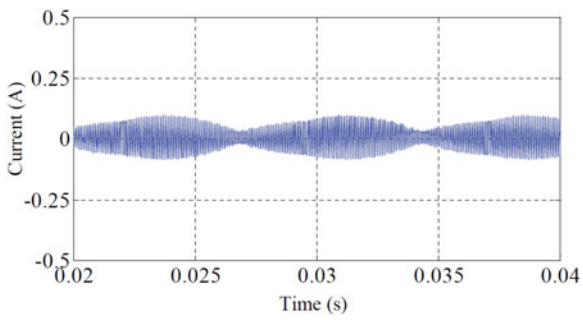

Fig. 15. Current estimation errors of phase A under ZVVSM (simulation results).

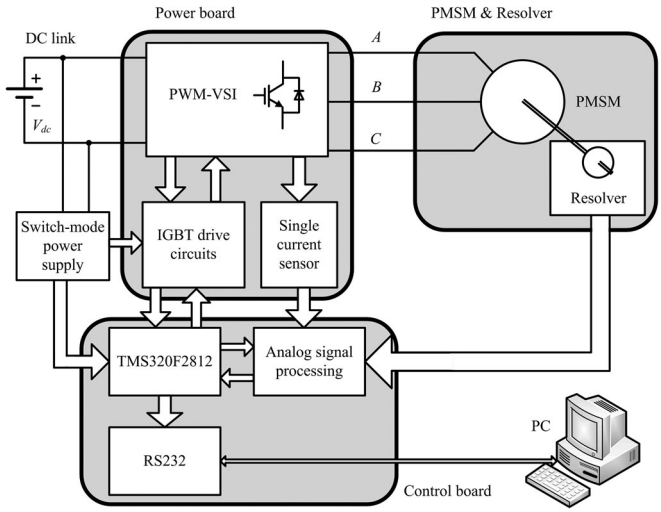

Fig. 16. Scheme of the experimental setup.

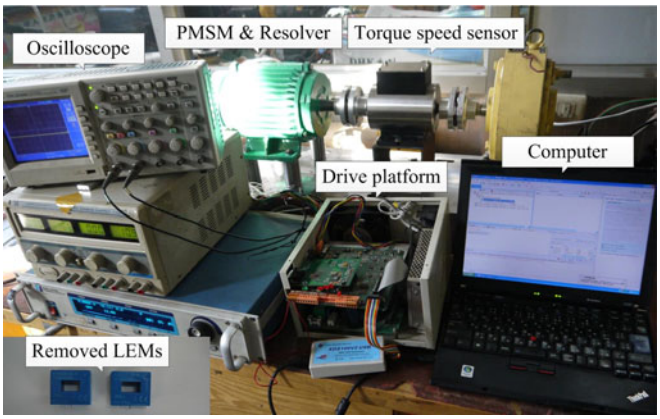

Fig. 17. Photograph of the experimental setup.

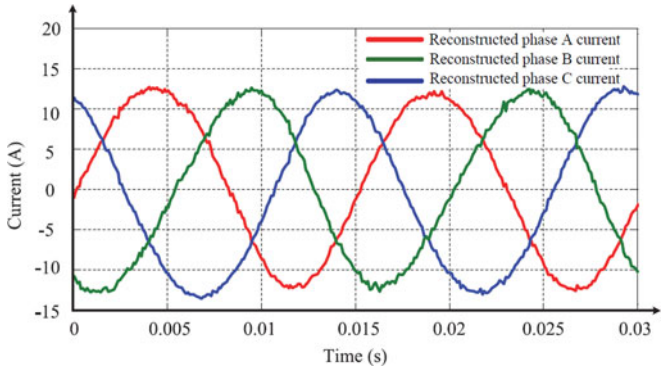

Fig. 18. Reconstructed three-phase currents under ZVVSM (experimental results).

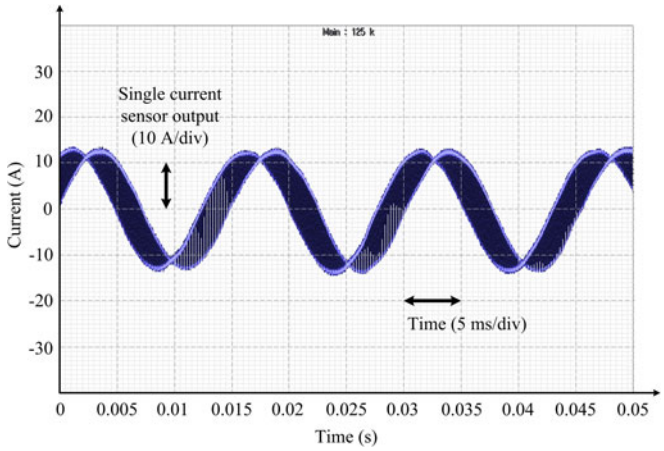

Fig. 19. Output of the single current sensor with the PWM frequency of 10 kHz (experimental results).

phase currents, the reconstruction errors are acceptable. So, the simulation results validate the proposed current reconstruction method.

V. Experimental Results

A. Experimental Setup

To further validate the proposed phase current reconstruction method, an experiment platform is set up, whose diagram and photograph are shown in Figs. 16 and 17, respectively. The experimental setup consists of a PWM-VSI, a PMSM with a resolver, a drive platform and a dc source. The PWM-VSI has a 3-kVA maximum power, a 10-kHz switching frequency of the IGBTs (IKW75N60T) and a 60-V dc-link nominal voltage. In the drive platform, a DSP, TMS320F2812, is used as the control unit to generate the PWM signals, sampling signals, and implement the proposed method. In this experimental setup, the minimum reliable current measurement time $T_{\min}$ is set at 5 μs. Moreover, motor parameters are shown in Table III. Furthermore, in order to ensure the accurate detection of the sample current, an isolated hall-effect current sensor (LEM HAIS-50P) with maximum sample rate 50 kHz is employed in this control system.

B. Experimental Results

Fig. 18 shows the experimental results of reconstructed three-phase currents under the ZVVSM. The motor speed is 1000 r/min and the load torque is 5 N·m, which are the same as the simulation setup. It can be seen that the three-phase sinusoidal currents are achieved. In the following experiments, the reconstructed currents are not only used for computing errors but also for control purposes. The control strategy is shown in Fig. 10, and the reconstructed three-phase currents are transformed to the *d–q* synchronous rotating frame, i_d and i_q, which are the feedback current signals of the current loops.

Fig. 19 gives the output of the single current sensor. It can be observed that the envelope curves of the current sensor output contain the information of the phase currents $-i_a$ and i_c. To clearly show the sampling points of ZVVSM, the output of the current sensor and the PWM signals are put in one figure. Fig. 20 shows the current sampling points and PWM signals during the two zero voltage vectors. In Fig. 20, it is obvious that the current sampling is occurred during the zero voltage vectors V_0 (000) and V_7 (111).

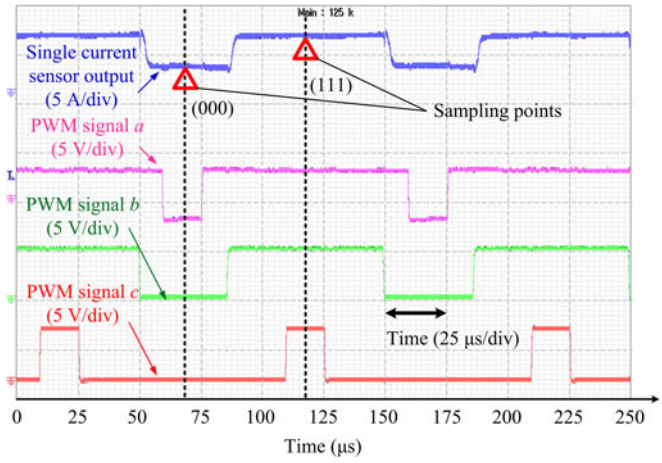

Fig. 20. Sampling points during the zero voltage vectors and PWM signals when the ZVVSM is adopted (experimental results).

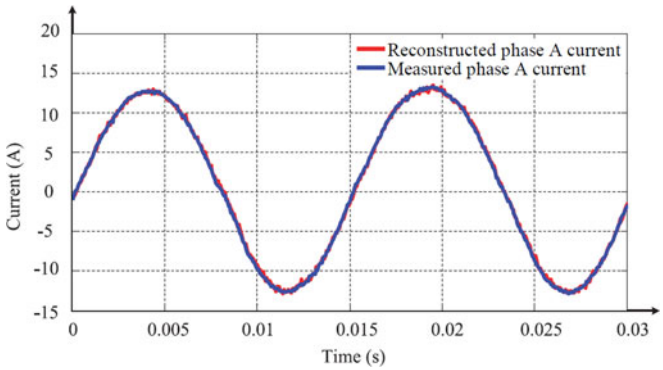

Fig. 21. Reconstructed and measured Phase A currents under ZVVSM (experimental results).

Fig. 21 shows the reconstructed and measured Phase A currents with the PWM frequency of 10 kHz when ZVVSM is adopted. Since there is no D/A converter in the experimental platform, the results of the reconstructed Phase A current are calculated in the DSP and real-time transmitted to the computer using the serial port RS232. Considering the transfer rate of RS232, the interrupt of RS232 is not triggered by the PWM. For comparison, the actual Phase A current is measured by another current sensor and also transmitted synchronously using the serial port RS232. Then, the results are plotted in one figure with MATLAB.

The current estimation errors are shown in Fig. 22. It can be seen that the reconstructed Phase A current is consistent with the actual measured phase A current and the current estimation errors are acceptable, which is about 3%. Nevertheless, there is difference between the simulation and experimental results. Furthermore, the low-frequency components of the experimental results are consistent with the motor electrical frequency and motor speed, which has the same changing law as the simulation results. Both in experimental and simulation results, the low-frequency components of error waveforms are caused by the ZVVSM algorithm, because the single current sensor output waveform is influenced by the values of the three-phase duty

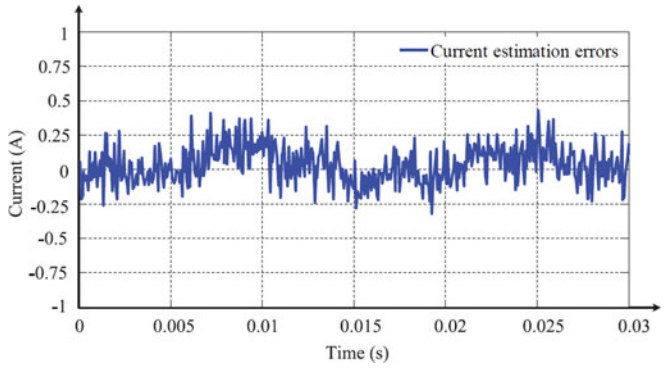

Fig. 22. Current estimation errors of Phase A under ZVVSM (experimental results).

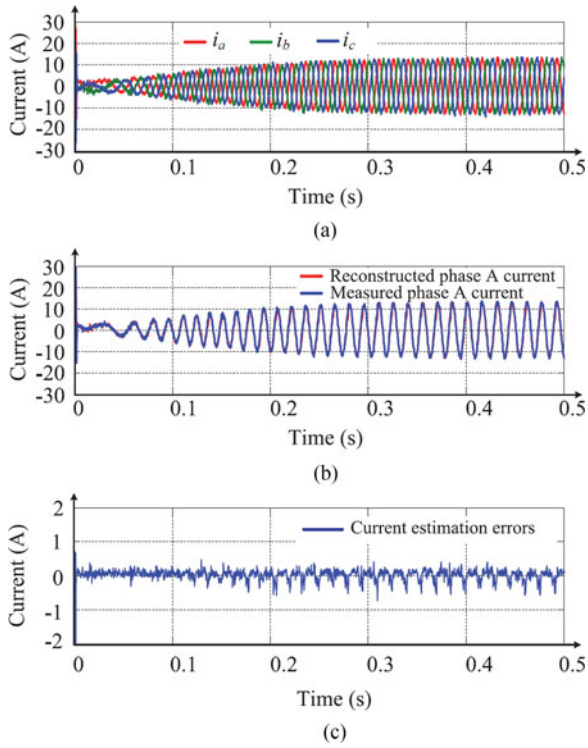

Fig. 23. Experimental results when the PMSM starts from standstill and accelerates to its rated speed (experimental results). (a) Reconstructed three-phase currents. (b) Reconstructed and measured Phase A currents. (c) Current estimation errors of Phase A.

cycles that are changed periodically with the motor electrical frequency. However, the high-frequency components of the error waveform in the experiment exist. The reason is that the two current sensors used for comparison are filtered separately by the filter circuits and transmitted to the DSP in the signal processing circuits of the drive platform. While in the simulation, this kind of influence factor does not exist. Besides, the features of the actual power switches and the electromagnetic interference in the whole control system are not considered in the simulation. As a result, the level of difference between simulation and experiment is mostly influenced by the measurement noise and the small difference of hardware circuits.

Moreover, to further prove the applicability of ZVVSM, an experiment is conducted, where the PMSM drive starts from

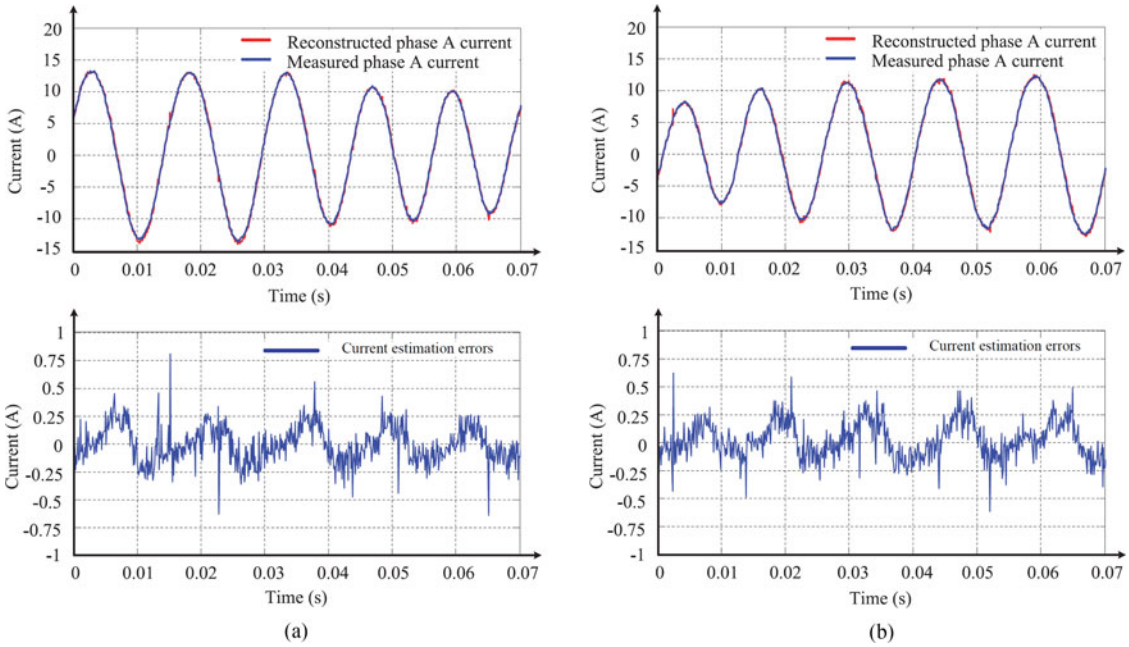

Fig. 24. Reconstructed and measured Phase A currents and the current estimation errors when the motor load is changing (experimental results). (a) Motor load is changed from the rated load 5 to 3 N·m (b) Motor load is changed from the 3 N·m back to rated load 5 N.m.

standstill and accelerates to its rated speed. Fig. 23 shows the experimental results of this starting process. Fig. 23(a) shows the reconstructed three-phase currents that are used for the current close-loop control. Fig. 23(b) shows the reconstructed and measured Phase A currents in this process, and Fig. 23(c) is the current estimation errors of Phase A. It is obvious that the current estimation errors become large with motor speed increasing. However, the errors are acceptable and the drive performance is not influenced too much.

Then, a variable load experiment under ZVVSM is carried out. The motor load is changed from the rated torque 5– 3 N·m and then back to 5 N·m. Fig. 24(a) and (b) show the experimental results when the motor load is decreasing and increasing, respectively. In the experiments, the modulation index is set as 0.8. The modulation index is defined as the ratio between the amplitude of the reference voltage vector and the inscribed circle radius of the space vector hexagon. According to the experimental results, the variable loads can cause the torque disturbances and influence the measurement results. Besides, there is a lot of error between the measured and reconstructed current at a certain instant. The reason is that the error can be influenced by the measurement noise. Moreover, when the motor is operating at variable loads, the torque disturbances can change the phase currents instantaneously during single PWM period. Then at a certain instant, the estimation errors of ZVVSM will become large. From the results it can be concluded that the reconstructed phase current is consistent with the actual measured phase current and the dynamic performance of ZVVSM is acceptable.

However, ZVVSM has some drawbacks on the fast current control dynamics if the phase currents change by as much as the rated value during single PWM period. To explain the reasons, the sampling principle of the ZVVSM should be analyzed. Since there is only one current sensor in the ZVVSM, it is impossible to obtain the three-phase currents at the same time. However, sampling phase currents at the same time is common in the conventional space vector control for PMSM by using two or more phase current sensors.

Therefore, in ZVVSM the three-phase currents should be reconstructed based on two samples recorded in different instants of the PWM period. If the motor speed is very high and the phase currents change by as much as the rated value during single PWM period, the estimation errors of ZVVSM will become large and the transient-related robustness will become inferior, which may limit the application range of ZVVSM. The aforesaid features are not the proprietary characteristics of ZVVSM, but they are also existed in other single current sensor methods. Owing to the sampling interval in these methods, the features in speed and transient-related robustness are general drawbacks among the single current sensor methods.

In all, the experimental results demonstrate that the proposed ZVVSM can reconstruct the phase currents accurately. A significant reason is that this method does not change the modulation mode of SVPWM, which is different from some other complicated algorithms using the single dc-link current sensor. So the ZVVSM can make the reconstructed phase currents with less waveform distortion and less harmonic contents, which are the advantages of this method.

VI. Conclusion

In this paper, a novel single current sensing technique, ZVVSM, is proposed for three-phase PMSM drive, which can move the dead zones toward the outline of the space vector hexagon without modifying PWM signal. This proposed method

is implemented by arranging the single current sensor at a novel position and the current can be sampled in the two zero voltage vectors. The dead zones and the maximum voltage utilization ratio of ZVVSM will decrease with the increase of the PWM frequency. There are some drawbacks in ZVVSM. First, compared with the typical single dc-link current sensor method, ZVVSM moves the dead zones toward the outline of the space vector hexagon, which limits the drive power and drive maximal speed. Second, since the wires between the two power switches should be led out, ZVVSM is not applicable to Integrated Power Modules. However, ZVVSM has the following merits which can compensate for its shortcomings.

1) There are no dead zones on the sector boundary. Furthermore, in ZVVSM the PWM waveforms do not need to be modified, which makes the control algorithm concise. As a result, the phase current waveforms are no longer influenced by the modification of PWM, which is beneficial to the PMSM drive performance.
2) In the ZVVSM, the PWM waveforms are not changed, which does not increase the switching times of the inverter during each PWM cycle. So the switching loss of the inverter will not increase and the drive system efficiency will not be influenced.
3) The ZVVSM removes the dead zones in the low modulation region, which makes this method is available and accurate at low motor speed.

Both simulation results and experimental results validate the effectiveness of the proposed phase current reconstruction method. Furthermore, the dynamic performance of ZVVSM is also verified by experiments. The ZVVSM is a suitable control strategy for low-cost and small-size PMSM drive applications.

REFERENCES

[1] W. Zheng, C. Jian, C. Ming, and K. T. Chau, "Field-oriented control and direct torque control for paralleled VSIs fed PMSM drives with variable switching frequencies," *IEEE Trans. Power Electron.*, vol. 31, no. 3, pp. 2417–2428, Mar. 2016.

[2] X. Yongxiang, Y. Qingbing, Z. Jinbin, Y. Yanmei, and Z. Guangqi, "Sinusoidal periodic carrier frequency modulation in reducing electromagnetic noise of permanent magnet synchronous motor," *IET Electr. Power Appl.*, vol. 7, pp. 223–230, 2013.

[3] X. Changliang, Z. Jiaxin, Y. Yan, and S. Tingna, "A novel direct torque and flux control method of matrix converter-fed PMSM drives," *IEEE Trans. Power Electron.*, vol. 29, no. 10, pp. 5417–5430, Oct. 2014.

[4] Q. Tengfei, W. Xuhui, and Z. Feng, "Adaptive-linear-neuron-based deadtime effects compensation scheme for PMSM drives," *IEEE Trans. Power Electron.*, vol. 31, no. 3, pp. 2530–2538, Mar. 2016.

[5] X. Ge, L. Kaiyuan, S. K. Dwivedi, J. R. Rosholm, and F. Blaabjerg, "Minimum-voltage vector injection method for sensorless control of PMSM for low-speed operations," *IEEE Trans. Power Electron.*, vol. 31, no. 2, pp. 1785–1794, Feb. 2016.

[6] N. Abou Qamar, C. J. Hatziadoniu, and W. Haibo, "Speed error mitigation for a DSP-based resolver-to-digital converter using autotuning filters," *IEEE Trans. Ind. Electron.*, vol. 62, no. 2, pp. 1134–1139, Feb. 2015.

[7] M. Seilmeier and B. Piepenbreier, "Sensorless control of PMSM for the whole speed range using two-degree-of-freedom current control and HF test current injection for low-speed range," *IEEE Trans. Power Electron.*, vol. 30, no. 8, pp. 4394–4403, Aug. 2015.

[8] X. Song, J. Fang, and B. Han, "High-precision rotor position detection for high-speed surface PMSM drive based on linear hall-effect sensors," *IEEE Trans. Power Electron.*, vol. 31, no. 7, pp. 4720–4731, Jul. 2016.

[9] M. Pacas, "Sensorless drives in industrial applications," *IEEE Ind. Electronics Mag.*, vol. 5, no. 2, pp. 16–23, Jun. 2011.

[10] L. Jarzebowicz, "Indirect measurement of motor current derivatives in PMSM sensorless drives," *Elektronika ir Elektrotechnika*, vol. 20, pp. 23–26, 2014.

[11] Y. Hua, M. Sumner, G. Asher, Q. Gao, and K. Saleh, "Improved sensorless control of a permanent magnet machine using fundamental pulse width modulation excitation," *IET Electr. Power Appl.*, vol. 5, pp. 359–370, 2011.

[12] T. C. Green and B. W. Williams, "Derivation of motor line-current waveforms from the DC-link current of an inverter," *Electr. Power Appl., IEE Proc. B*, vol. 136, pp. 196–204, 1989.

[13] Y. Shih-Chin, "Saliency-based position estimation of permanent-magnet synchronous machines using square-wave voltage injection with a single current sensor," *IEEE Trans. Ind. Appl.*, vol. 51, no. 2, pp. 1561–1571, Mar./Apr. 2015.

[14] F. Blaabjerg, J. K. Pedersen, U. Jaeger, and P. Thoegersen, "Single current sensor technique in the DC link of three-phase PWM-VS inverters: A review and a novel solution," *IEEE Trans. Ind. Appl.*, vol. 33, no. 5, pp. 1241–1253, Sep./Oct. 1997.

[15] L. Woo-Cheol, H. Dong-seok, and L. Taeck-Kie, "A novel control method for three-phase PWM rectifiers using a single current sensor," *IEEE Trans. Power Electron.*, vol. 15, no. 5, pp. 861–870, Sep. 2000.

[16] L. Yen-Shin, L. Yong-Kai, and C. Chih-Wei, "New hybrid pulsewidth modulation technique to reduce current distortion and extend current reconstruction range for a three-phase inverter using only DC-link sensor," *IEEE Trans. Power Electron*, vol. 28, no. 3, pp. 1331–1337, Mar. 2013.

[17] L. Woo-Cheol, L. Taeck-Kie, and H. Dong-seok, "Comparison of single-sensor current control in the DC link for three-phase voltage-source PWM converters," *IEEE Trans. Ind. Electron.*, vol. 48, no. 3, pp. 491–505, Jun. 2001.

[18] B. Saritha and P. A. Janakiraman, "Sinusoidal three-phase current reconstruction and control using a DC-link current sensor and a curve-fitting observer," *IEEE Trans. Ind. Electron.*, vol. 54, no. 5, pp. 2657–2664, Oct. 2007.

[19] H. Jung-Ik, "Voltage injection method for three-phase current reconstruction in PWM inverters using a single sensor," *IEEE Trans. Power Electron.*, vol. 24, no. 3, pp. 767–775, Mar. 2009.

[20] K. Hongrae and T. M. Jahns, "Current control for ac motor drives using a single dc-link current sensor and measurement voltage vectors," *IEEE Trans. Ind. Appl.*, vol. 42, no. 6, pp. 1539–1547, Nov./Dec. 2006.

[21] K. Hongrae and T. M. Jahns, "Phase current reconstruction for ac motor drives using a dc link single current sensor and measurement voltage vectors," *IEEE Trans. Power Electron.*, vol. 21, no. 5, pp. 1413–1419, Sep. 2006.

[22] G. Yikun, N. Fenglei, Y. Dapeng, and L. Hong, "Switching-state phase shift method for three-phase-current reconstruction with a single DC-link current sensor," *IEEE Trans. Ind. Electron.*, vol. 58, no. 11, pp. 5186–5194, Nov. 2011.

[23] H. Jung-Ik, "Current prediction in vector-controlled pwm inverters using single DC-link current sensor," *IEEE Trans. Ind. Electron.*, vol. 57, no. 2, pp. 716–726, Feb. 2010.

[24] S. Kai, Q. Wei, H. Lipei, and K. Matsuse, "An overmodulation method for PWM-inverter-fed IPMSM drive with single current sensor," *IEEE Trans. Ind. Electron.*, vol. 57, no. 10, pp. 3395–3404, Oct. 2010.

[25] L. Haifeng *et al.*, "A three-phase current reconstruction technique using single DC current sensor based on TSPWM," *IEEE Trans. Power Electron.*, vol. 29, no. 3, pp. 1542–1550, Mar. 2014.

[26] B. Hafez, A. S. Abdel-Khalik, A. M. Massoud, S. Ahmed, and R. D. Lorenz, "Single-sensor-based three-phase permanent-magnet synchronous motor drive system with Luenberger observers for motor line current reconstruction," *IEEE Trans. Ind. Appl.*, vol. 50, no. 4, pp. 2602–2613, Jul./Aug. 2014.

[27] Y. Haizhong and A. Emadi, "A six-phase current reconstruction scheme for dual traction inverters in hybrid electric vehicles with a single dc-link current sensor," *IEEE Trans. Veh. Technol.*, vol. 63, no. 7, pp. 3085–3093, Sep. 2014.

[28] M. Carpaneto, P. Fazio, M. Marchesoni, and G. Parodi, "Dynamic performance evaluation of sensorless permanent-magnet synchronous motor drives with reduced current sensors," *IEEE Trans. Ind. Electron.*, vol. 59, no. 12, pp. 4579–4589, Dec. 2012.

[29] L. Jarzebowicz, A. Opalinski, and M. Cisek, "Improving control dynamics of PMSM drive by estimating zero-delay current value," *Elektronika ir Elektrotechnika*, vol. 21, pp. 20–23, 2015.

Yongxiang Xu (M'03) was born in Guangxi Province, China, in 1977. He received the M.S. and Ph.D. degrees in electrical engineering from the Harbin Institute of Technology, Harbin, China, in 2001 and 2005, respectively.

He is currently a Professor in the State Key Laboratory of Robotics and System, Harbin Institute of Technology. His current research interests include permanent-magnet machine design and control.

Hao Yan (S'16) was born in Liaoning, China, in 1989. He received the B.S. and M.S. degrees in electrical engineering, in 2011 and 2013, respectively, from the Harbin Institute of Technology, Harbin, China, where he is currently working toward the Ph.D. degree.

His current research interests include power converter and permanent-magnet motor drives.

Jibin Zou (SM'00) was born on January 19, 1957, in Heilongjiang Province, China. He received the M.S. and Ph.D. degrees in electrical engineering from the Harbin Institute of Technology, Harbin, China, in 1984 and 1988, respectively.

Since 1985, he has been engaged in the research in electrical machines. He was with the University of Liverpool, Liverpool, U.K., as a Visiting Research Fellow for one year. He is currently a Professor in the State Key Laboratory of Robotics and System, Harbin Institute of Technology.

Dr. Zou has been a Senior Member of the IEEE Magnetics Society, since 2000. His current research interests include permanent-magnet machine design and control.

Baochao Wang (M'16) received the B.S. and M.S. degrees from the Harbin Institute of Technology (HIT), Harbin, China, in 2008 and 2010, respectively, and the Ph.D. degree from the University of Technology of Compiegne, Compiegne, France, in 2014, all in electrical engineering.

Since 2014, he has been a Lecture in the Department of electrical Engineering, HIT. His current research interests include PMSM drive and control, renewable energy integration, and power quality.

Yunhui Li was born in Heilongjiang Province, China, in 1989. He received the B.S. and M.S. degrees in electrical engineering from the Harbin Institute of Technology, Harbin, China, in 2012 and 2014, respectively.

He is currently at the Changchun Institute of Optics, Fine Mechanics and Physics, Chinese Academy of Sciences, Changchun, China.